Unexpected ion exchange between NH4+ and CuII ions in Cu-CHA zeolites upon formation of the [CuII2(NH3)4O2]2+ peroxo complex

Microporous and Mesoporous Materials 405 (2026) 114075

Contents lists available at ScienceDirect

Microporous and Mesoporous Materials

journal homepage: www.elsevier.com/locate/micromeso

Unexpected ion exchange between NH_4^+ and Cu^{II} ions in Cu-CHA zeolites upon formation of the $[Cu_2^{II}(NH_3)_4O_2]^{2+}$ peroxo complex

Stefano Magliocco [a,1], Reza K. Abasabadi [a,b,2], Francesco D'Amico [c], Joachim D. Bjerregaard [d,e], Anastasia Yu Molokova [f], Henrik Grönbeck [d], Ton V.W. Janssens [b], Gloria Berlier [a,*]

[a] Department of Chemistry, NIS Centre and INSTM Reference Centre, University of Turin, via Giuria 7, 10125, Turin, Italy
[b] Umicore Denmark ApS, c/o Umicore AG & Co KG, Rodenbacher Chaussee 4, 63547, Hanau, Germany
[c] Elettra-Sincrotrone Trieste S.C.p.A., Strada Statale 14 – km 163, TS, 5 in AREA Science Park, Basovizza, 34149, Italy
[d] Department of Physics and Competence Centre for Catalysis, Chalmers University of Technology, SE-412 96, Göteborg, Sweden
[e] Umicore AG & Co. KG, Rodenbacher Chaussee 4, 63457, Hanau, Germany
[f] ALBA Synchrotron, Carretera BP 1413, Km 3, 3, Barcelona, 08290, Spain

A B S T R A C T

In this work, we have followed by *in situ* IR spectroscopy the stepwise formation of the $[Cu_2^{II}(NH_3)_4O_2]^{2+}$ peroxo complex in Cu-CHA zeolites with different Cu loading and Si/Al ratios. Unexpected changes were observed while oxidizing the $[Cu^{I}(NH_3)_2]^{+}$ complexes formed by reaction of Cu-CHA with an NO/NH_3 mixture. Namely, this process, causes a decrease in the intensity of physisorbed NH_3 (bending mode at 1620 cm^{-1}) and of its protonated form, NH_4^+ (bending mode at 1434 cm^{-1}). These changes are correlated with the increase of a band at 900 cm^{-1}, which is coherent with the growth of framework coordinated Z_2Cu^{II} sites, where Z represent a negative charge on the framework, as confirmed by DFT calculations. The process can be described as an ion exchange between NH_4^+ and Cu^{II} ions during the oxidation, with formation of H_2O and removal of protons. More Cu^{II} ions are replacing NH_4^+ at high Cu loading and low Si/Al ratio, in agreement with the current understanding of the effect of these parameters on ions diffusion, which in turns affect the efficiency of the oxidation and reduction half cycles of Cu-CHA in the low temperature NH_3-SCR reaction.

1. Introduction

Cu-CHA zeolites have been extensively investigated in the last decade in relation to their excellent performance and stability as catalysts for the NH_3-mediated selective catalytic reduction (NH_3-SCR), the basis for the deNOx technologies used in the aftertreatment of exhaust gases in diesel vehicles [1]. This outstanding performance, coupled with the structural simplicity of the CHA topology, caused a boom of academic and industrial research groups focusing on the fascinating chemistry involved in the reaction, involving kinetic measurements, DFT calculations, transient-response methods and spectroscopic studies [2–11].

A common understanding is that the NH_3-SCR reaction, where NO is reduced by NH_3 in the presence of O_2 to give N_2 and H_2O, involves a redox cycle where Cu ions alternate between the Cu^{II} and Cu^{I} oxidation state. The reaction can be thus studied by dividing the catalytic cycle into one reduction half cycle (RHC, where Cu^{II} ions are reduce to Cu^{I} by NO and NH_3, releasing N_2 and H_2O), and one oxidation half-cycle (OHC), which restores the Cu^{II} site [3,4,12,13]. A breakthrough was the observation that at low temperature (below 250 °C) Cu^{II} and Cu^{I} ions are solvated by NH_3 and show some mobility inside the zeolite cages, placing the reaction at the interface between homogenous and heterogenous catalysis [10,12,14–16]. In these conditions, the reaction can be described in terms of pairs of mobile $[Cu^{I}(NH_3)_2]^{+}$ complexes formed in the RHC, reacting with O_2 to form an oxygen-bridged, amino-solvated dicopper complex, with formula $[Cu_2^{II}(NH_3)_4O_2]^{2+}$ [15]. X-ray Absorption Spectroscopy (XAS) coupled to DFT calculations established the structure of the complex as a μ-η^2,η^2-peroxo diamino dicopper (II) [5,12,15,17–19].

Even if in an NH_3 atmosphere the Cu ions (both Cu^{II} and Cu^{I}) are solvated and potentially mobile, they are still electrostatically tethered to the framework negative charges [4]. As a consequence, their mobility

* Corresponding author.
E-mail address: gloria.berlier@unito.it (G. Berlier).
[1] Present address: Dipartimento di Ingegneria Elettronica, Chimica ed Ingegneria Industriale, University of Messina, V.le F. Stagno D'Alcontres 31, 98,166 Messina, Italy.
[2] Present address: Department of Chemistry, Danmarks Tekniske Universitet, Kemitorvet, 2800 Kgs. Lyngby, Denmark.

https://doi.org/10.1016/j.micromeso.2026.114075
Received 18 December 2025; Received in revised form 29 January 2026; Accepted 3 February 2026
Available online 7 February 2026

is affected by their charge and by the density (Si/Al ratio) and spatial distribution of framework Al heteroatoms [20–23]. Moreover, the exchange of CHA zeolites with Cu^{II} ions is never complete, thus the zeolite also exposes Si-(OH)-Al Brønsted acid sites which protonate NH_3 forming NH_4^+ ions. In principle, the steric hindrance of NH_4^+ ions can have a potential blocking effect on the migration of NH_3-solvated Cu complexes. However, Molecular Dynamic simulations indicate that NH_4^+ ions influence the long range migration of $[Cu^I(NH_3)_2]^+$ by their simultaneous displacement for charge compensation, and that migration is favored by proton transfer from NH_4^+ to NH_3, when the latter is in excess [21].

The changes in the oxidation and coordination state of Cu ions during the interaction with the NH_3-SCR mixture (NH_3, NO, O_2) have been studied by different spectroscopic techniques such as XAS and EPR [8,17,24,25]. Infrared spectroscopy has been used via time-resolved transient experiments or by the modulation excitation approach to detect key transient reaction intermediates [9,26], or to follow the formation and reactivity of Cu^{II}-(N,O) species in steady state conditions [18,27,28]. IR spectroscopy also provides direct information on the concentration of surface Si-OH and Brønsted acid sites by analysis of their OH stretching frequency (νOH), and on the presence of NH_3 ligands and NH_4^+ groups [14,29–31]. Indirect information on the presence and relative amount of framework coordinated Cu ions (Z_2Cu^{II}, $ZCu^{II}OH$, ZCu^I etc, where Z represents the negative charge on the framework generated by the presence of the Al heteroatom) can be obtained from the perturbation of the $[TO_4]$ zeolite building blocks (T = Si or Al) stretching vibrations in the so-called silica window between 1000 and 800 cm^{-1} [30–36].

In the OHC reaction described above, that is:

$$2\ [Cu^I(NH_3)_2]^+ + O_2 \rightarrow [Cu^{II}_2(NH_3)_4O_2]^{2+} \quad (1)$$

IR spectroscopy is not supposed to show appreciable changes, since: i) both Cu species are NH_3 solvated and thus should not cause perturbation of $[TO_4]$ framework vibrations [34,35]; ii) the overall number of NH_3 ligands does not change; iii) the overall charge does not change, implying that NH_4^+ and Brønsted acid sites groups should not be involved in the reaction for charge compensation.

In this contribution, we have followed reaction (1) by infrared spectroscopy as a preliminary step to study the poisoning by SO_2 of Cu-CHA zeolites in the NH_3-SCR reaction [37–39]. Surprisingly, we observed unexpected and reproducible changes in the NH_3, NH_4^+ and Z_2Cu^{II} vibrational fingerprints during the reaction, with a dependence on both Cu content and Si/Al ratio. To interpret the observed changes, we applied DFT to calculate the vibrational fingerprint of framework coordinated and NH_3-solvated Cu ions in the silica window. The observed changes are thus rationalized in terms of ion exchange between NH_4^+ and Cu^{II} during the reaction. Another explanation would involve the formation of nitrite-like species (HONO) during the RHC, as proposed based on transient response methods and chemical trapping [40,41], which would then be oxidized during the OHC. The possible impact of these observations on Cu-ion mobility in Cu-CHA zeolites is discussed [42].

2. Experimental

Two Cu-CHA zeolites with Cu content of 3.2 wt% and Si/Al ratio 6.7 and 15 (Cu/Al = 0.32 and 0.62 respectively), and one Cu-CHA with Cu content of 0.8 wt% and Si/Al ratio 6.7 (Cu/Al = 0.08) were prepared by ion exchange as described elsewhere [37]. Fourier Transform IR spectra were measured in transmission mode on pelletized samples using a Bruker Invenio spectrophotometer equipped with an MCT detector. Spectra were acquired with a resolution of 2 cm^{-1} accumulating 32 scans.

In situ IR measurements were carried out with the 'Sandwich' IR reactor cell described in Ref. [43], which allows measurements under controlled temperature and reactant flow conditions. The flow system comprehends bottles of O_2, N_2, 2055 ppm NO in N_2, 1700 ppm NH_3 in N_2. The fluxes have been regulated with Brooks Instruments mass flows controllers.

In all experiments the zeolites were first heated at 300 °C in O_2 and left at this temperature for 1 h before cooling to 200 °C in the same atmosphere (step 1). At this temperature they were exposed to NO/NH_3 (500 ppm/600 ppm in N_2) for 1 h, resulting in the formation of mobile $[Cu^I(NH_3)_2]^+$ complexes (RHC, step 2) [5,12,15–17], followed by exposure to 10% O_2 in N_2 for 1 h to form the formation of $[Cu^{II}_2(NH_3)_4O_2]^{2+}$ complexes (OHC, step 3). A 20 min N_2 purge was carried out between each of the described steps. Total flow: 100 ml/min for step 1 and N_2 flush, 50 ml/min for steps 2-3. A protocol scheme is summarized in Fig. S1 in Supporting Information.

Spin-polarized density functional theory (DFT) was used to calculate the structure and vibrational fingerprints of framework coordinated and NH_3-solvated Cu ions in Cu-CHA, using the Vienna Ab initio Simulation package (VASP) version 5.4.4 [44,45]. The Kohn-Sham orbitals were expanded with plane waves and the cutoff was set to 480 eV. The Perdew-Burke_Ernzerhof (PBE) functional [46] was used to approximate the exchange-correlation term. To account for van deer Waals interactions, the Grimme D3 correction [47] was augmented, and a Hubbard term [48] of 6 eV was applied to describe the localized Cu 3d electrons. The interaction between the core and valence electrons were described with the plane augmented wave (PAW) [49,50]. The valence electrons considered for each atom were Cu(11), Si(4), Al (3), O (6), N (5) and H (1).

The k-point sampling was restricted to the gamma point. The converging criteria for the SCF loop was set to 10^{-5} eV and the structures were considered a minimum if the norm of all forces was less than 0.02 eV/Å. Vibrational analysis was performed along with the calculation of IR intensities. The IR analysis was carried out by performing a vibrational analysis using density functional perturbation theory (DFPT) with the IR intensities computed using the VASP-infrared code [51]. For Raman intensities, the vibrational analysis was performed using the finite difference method with the Raman intensities computed using the VASP-Raman script [52]. The chabazite structure was modelled using the rhombohedral unit cell (9.36 Å, 9.40 Å, 9.42 Å), with 12 Si atoms. When Cu ions were introduced into the system either one or two Si atoms were exchanged with an Al atom, giving a Si/Al ratio of 11.

The calculated frequencies were scaled by a factor of 1.056 to take into account the anharmonic effects [53]. The scale factor has been obtained using a reference compound, namely crystalline $(NH_4)_2SO_4$, and comparing its calculated spectrum with the experimental Raman one (see SI, Fig. S2). The final simulated IR spectra were obtained as a sum of Voigt curves, centered at the calculated frequencies, with relative areas proportional to the IR intensities, both Gaussian and Lorentzian Full Widths at Half Maximum (FWHM) were set to 10 cm^{-1}, as done in Ref. [54].

3. Results

3.1. Formation of the $[Cu^{II}_2(NH_3)_4O_2]^{2+}$ peroxo complex

In situ IR spectroscopy has been used to follow the different steps to obtain the $[Cu^{II}_2(NH_3)_4O_2]^{2+}$-peroxo complex on three Cu-CHA zeolite-based catalysts with different Cu content and Si/Al ratio. We will first discuss in detail the different steps for the zeolite with Cu/Al = 0.32 and Si/Al = 6.7 and then analyse the effect of Si/Al and of Cu content.

The spectrum can be divided into three regions (Fig. 1): i) the NH and OH stretching region (νNH and νOH, between 3000 and 400 cm^{-1}); ii) the region between 1700 and 1350 cm^{-1}, characteristic of the bending modes of NH_3 and NH_4^+ (δNH_3 and δNH_4^+); iii) the silica window (1000 - 800 cm^{-1}), an IR transparent region between the intense $[TO_4]$ asymmetric and symmetric stretching vibrations (ν_{asym} and ν_{sym}) [32].

In the first region (Fig. 1a), the intense band at 3606 with a shoulder

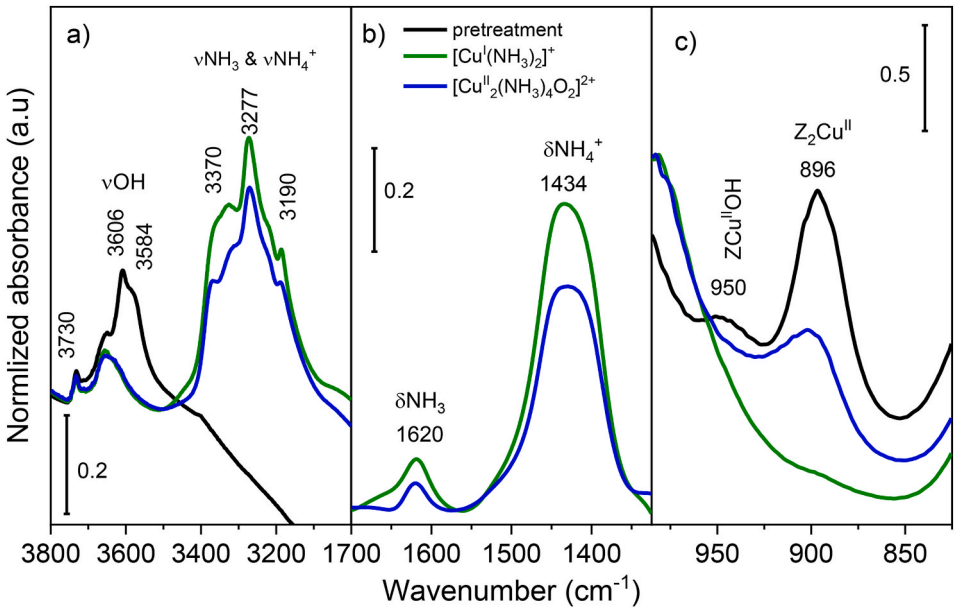

Fig. 1. FTIR spectra of Cu-CHA with Cu/Al = 0.32 and Si/Al = 6.7 in the a) νOH, b) $\delta NH_3/\delta NH_4^+$ and c) silica window regions during different steps of the procedure: 1) pretreatment in O_2 (black), 2) reduction with NO/NH_3 mixture (RHC, 500 ppm/600 ppm in N_2, green), 3) subsequent oxidation with O_2 10% in N_2 (OHC, blue). The spectra displayed in panel b) are background subtracted, using the spectrum measured before NO/NH_3 dosage as a reference. All spectra measured at 200 °C after N_2 flush. (For interpretation of the references to color in this figure legend, the reader is referred to the Web version of this article.)

at 3584 cm^{-1} correspond to the Brønsted acid sites in the CHA structure, that have not been exchanged by Cu ions [26,48,55]. At higher frequency, weaker band are founds at 3730 cm^{-1} assigned to the internal SiOH [50] and a shoulder around 3650 cm^{-1}. The latter could be assigned to $ZCu^{II}OH$ species [56] or to Al-OH species on defective extraframework or partially extraframework Al atoms in distorted tetrahedral coordination [36,57,58]. The low Si/Al ratio of this material suggests that the predominant species are Al-OH.

In Fig. 1c the silica window is depicted. Two bands appear which have been explained in terms of the ν_{asym} vibrations of the $[TO_4]$ units perturbed by the presence of framework coordinated Cu^{II} ions [32]. The more intense band, located at 896 cm^{-1}, is associated with Z_2Cu^{II} in the 6-membered ring of the zeolite, and the less intense band at 950 cm^{-1} to $ZCu^{II}OH$ in the 8-membered ring [10,31]. The relative intensity of the two bands reflects the $Z_2Cu^{II}/ZCu^{II}OH$ relative abundance expected on the basis of the catalyst Cu/Al and Si/Al ratio [31,33,35,59].

In step 2 a mixture of NO/NH_3 in N_2 was dosed on the catalyst at 200 °C to produce the $[Cu^{I}(NH_3)_2]^+$ complexes in the RHC [12,14]. Evidence for their formation is the appearance of the band at 1620 cm^{-1}, which is related to the δNH_3 vibration of the ligand NH_3 in the $[Cu^{I}(NH_3)^+]$ complex, and the disappearance of the bands at 896 and 950 cm^{-1} (Fig. 1b and c, respectively) as a consequence of the reduction and solvation of framework Cu^{II} ions [34]. The presence of NH_3 in the flow also results in the formation of NH_4^+ (δNH_4^+ at 1434 cm^{-1}, panel b) by reaction with Brønsted acid sites as indicated by the loss of intensity around 3600 cm^{-1} (panel a). The IR signals of the corresponding NH stretching (νNH) of NH_3 and NH_4^+ overlap in the high frequency region, giving a sharp peak at 3277 cm^{-1} with shoulders at 3370 and 3190 cm^{-1} [60–62]. Only minor changes are observed concerning Si-OH groups (band at 3730 cm^{-1}) and Al-OH groups on extraframework Al atoms (3650 cm^{-1}), in agreement with their low Brønsted acid strength [63]. As an additional comment, we acknowledge a high frequency shoulder in the band related to NH_3, around 1664 cm^{-1}. This could be the weaker bending mode of NH_4^+ and/or could involve the contribution of the νN=O of HONO (often reported for cis-HONO near 1660 cm^{-1}) [62]. The latter hypothesis is less likely, since HONO is supposed to be a labile species, quickly reacting with NH_3 [4]. The resulting nitrite species, if formed in the present experimental conditions, cannot be observed by infrared spectroscopy on zeolites, since the characteristic bands fall in the 1470–1050 cm^{-1} range, which in Cu-CHA is fully overshadowed by the more intense asymmetric stretching modes of the zeolite framework [27].

Both phenomena (coordination of NH_3 to Cu ions and formation of NH_4^+ ions) are relatively fast reaching 80/90% of their maximum evolution in the first 3 min (see Figs. S3 and S4). The decrease in the band related to Z_2Cu^{II} (896 cm^{-1}) shows a similar trend with time-on-stream, while the $ZCu^{II}OH$ one (950 cm^{-1}) is only affected after 2.5 min, which corresponds to a small burst in the intensity of NH_3 and NH_4^+ (Fig. S4). This would suggest a faster reactivity of NH_3 with the Z_2Cu^{II} sites with respect to $ZCu^{II}OH$, which starts to be solvated only after the former is saturated.

Oxidation in $10\%O_2/N_2$ (OHC) of the $[Cu^{I}(NH_3)_2]^+$ complexes at 200 °C results in the formation of the $[Cu^{II}_2(NH_3)_4(O_2)]^{2+}$ complexes. In the IR spectra, this reaction is visible by a decrease of the NH_3 and NH_4^+ bands, and a concomitant growth in the silica window of a band with maximum at 900 cm^{-1} (panels b and c, respectively). The former is slightly shifted and broadened with respect to the Z_2Cu^{II} band in the pretreated catalyst and indicates the coordination of Cu ions to the framework along with the formation of the $[Cu^{II}_2(NH_3)_4(O_2)]^{2+}$ complexes. There are no further significant changes in the bands related to Brønsted sites (Fig. S5).

To investigate the nature of these changes, we have followed the evolution with time of the bands intensity (Fig. 2). Both bands at 1434 (δNH_4^+) and at 900 cm^{-1} show an abrupt decrease/increase in the first few minutes of the reaction, while the δNH_3 band at 1620 cm^{-1} decreases more gradually. After this period, the intensity of δNH_4^+ reaches a plateau, while the δNH_3 and 900 cm^{-1} bands continue to gradually decrease and increase, respectively. This suggests that the fast growth of the band at 900 cm^{-1} in the first minutes is related to the decrease of NH_4^+, and that the further evolution is related to the desorption of coordinated NH_3.

To check the reversibility and reproducibility of the observed trends, the $[Cu^{II}_2(NH_3)_4O_2]^{2+}$ complex was reduced to $[Cu^{I}(NH_3)_2]^+$ by reaction with NO/NH_3, followed by an oxidation step at 200 °C [18,37]. Fig. 3 shows that the evolution of the bands at 1620, 1434, and 900 cm^{-1} closely follows the reduction–oxidation sequence. During the reduction

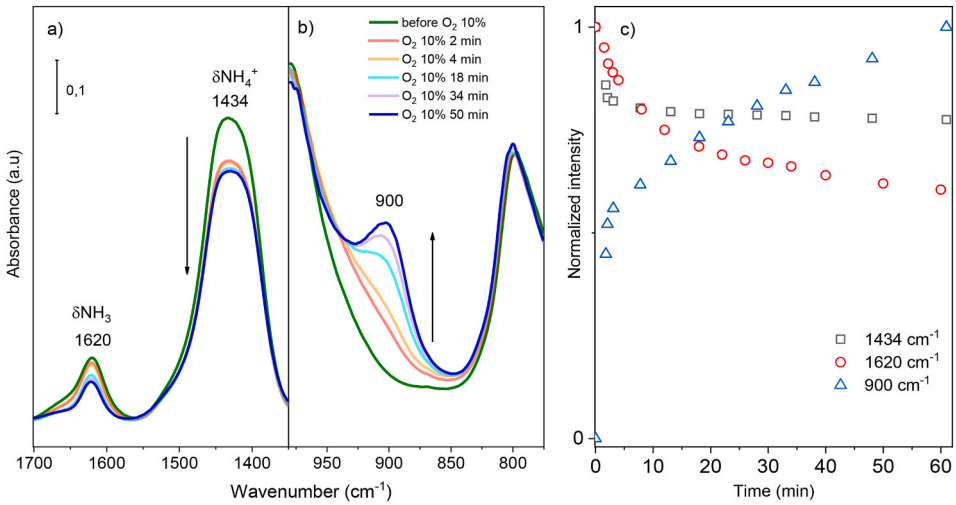

Fig. 2. Evolution with time of the infrared spectra in the a) νOH and b) silica window regions measured on Cu-CHA with Cu/Al = 0.32 and Si/Al = 6.7 during the exposure of $[Cu^{I}(NH_3)_2]^+$ complexes to O_2 (OHC). c) Plot of the corresponding normalized intensity vs time. The intensity has been normalized with respect to the initial and final intensity for $\delta NH_3/\delta NH_4^+$ and 900 cm^{-1} bands, respectively.

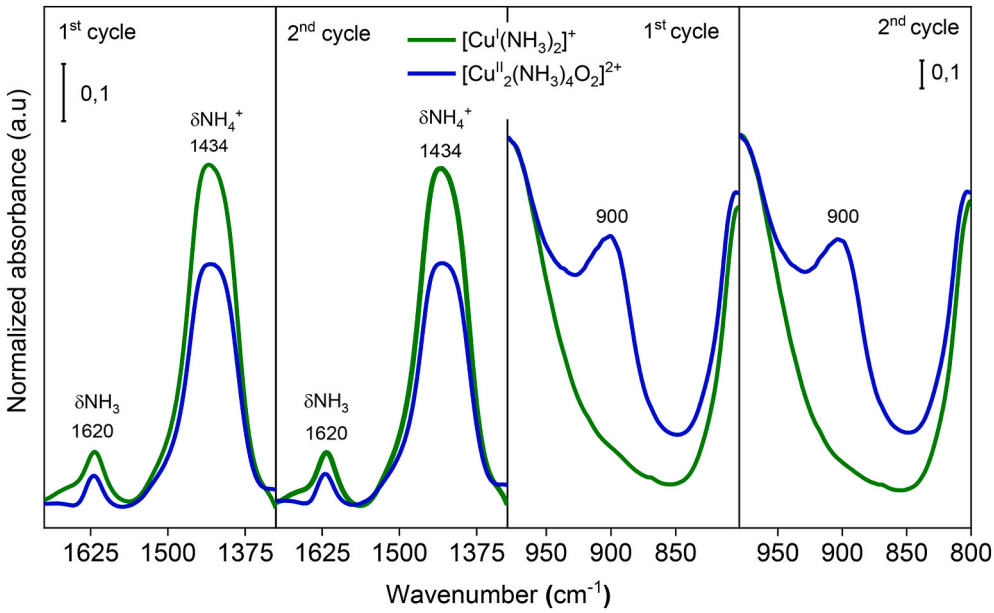

Fig. 3. *R*eproducibility of the NO/NH_3 reduction (RHC, 500 ppm/600 ppm in N_2, green) and 10% O_2 in N_2 oxidation (OHC, blue) cycles at 200°C on Cu-CHA with Cu/Al = 0.32 and Si/Al = 6.7, measured in two successive cycles. FTIR spectra in the $\delta NH_3/\delta NH_4^+$ and silica window regions (left and right panels, respectively). Spectra in the $\delta NH_3/\delta NH_4^+$ region are background subtracted, using the spectrum measured before NO/NH_3 dosage as a reference. All spectra measured at 200 °C after N_2 flush. (For interpretation of the references to color in this figure legend, the reader is referred to the Web version of this article.)

step, the bands at 1620 and 1434 cm^{-1} associated with the $[Cu^{I}(NH_3)_2]^+$ complex are fully restored. Upon re-oxidation, the band at 900 cm^{-1} re-emerges, while the intensity of the 1620 and 1434 cm^{-1} bands decreases, as observed during the formation of the $[Cu^{II}_2(NH_3)_4(O_2)]^{2+}$ complex in the first cycle.

In the reduced state of the Cu-CHA catalyst (Cu/Al = 0.32, Si/Al = 6.7, $[Cu^{I}(NH_3)_2]^+$ complexes), the integrated area of the bands centered at 1620 and 1434 cm^{-1} is higher by *ca* 62 and 32%, respectively, compared to the oxidized state at 200 °C, where $[Cu^{II}_2(NH_3)_4(O_2)]^{2+}$ complexes are present. The integrated area of the band at 900 cm^{-1} cannot be measured with decent accuracy, being related to a perturbation of the framework $[TO_4]$ vibrations [32].

3.2. *Effect of zeolite composition*

The same set of experiments was carried out on a Cu-CHA catalyst with Cu/Al = 0.62 and Si/Al = 15, having a higher Si/Al ratio, but the same Cu wt% content, and on a catalyst with a lower Cu content (0.8 wt %, Cu/Al = 0.08 and Si/Al = 6.7). We focus our attention on the δNH_3 (1620 cm^{-1}) and δNH_4^+ (1434 cm^{-1}) bands and the silica window (Fig. 4). The spectra have been normalized with respect to the pellet thickness. They are reported in the same vertical scale as Fig. 1 for Cu-CHA with Cu/Al = 0.08 and Si/Al = 6.7 (panels c and d), while the vertical scale for the Cu-CHA with Cu/Al = 0.62 and Si/Al = 15 is halved, compared the Si/Al = 6.7 catalysts.

The effect of the Si/Al ratio is evident in the silica window (panel b). In contrast to the catalyst with Si/Al = 6.7 and the same Cu content (Fig. 1), after the pretreatment in O_2 (black curve) we now observe 2

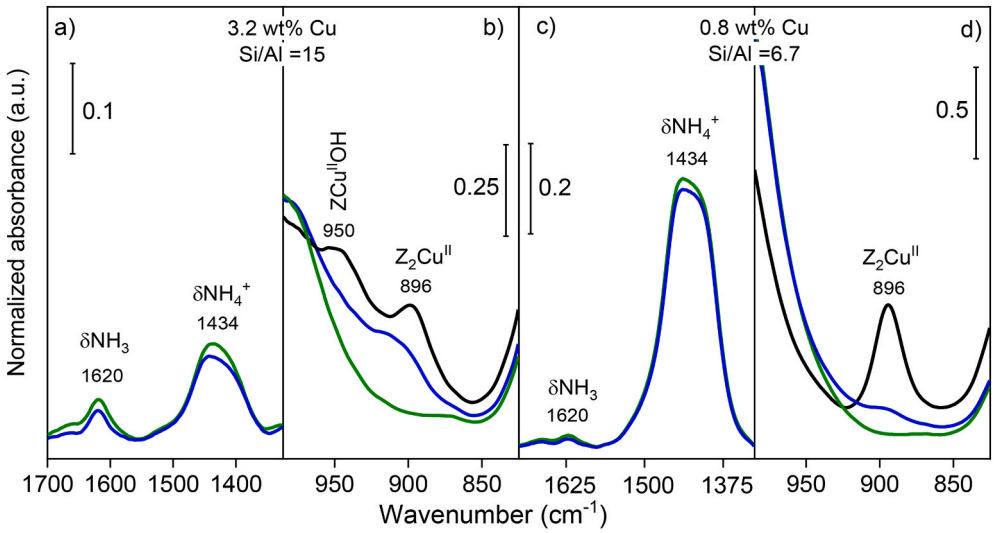

Fig. 4. Effect of the composition: FTIR spectra of Cu-CHA with Cu/Al = 0.62 and Si/Al = 15 (a, b) and of Cu-CHA with Cu/Al = 0.08 and Si/Al = 6.7 (c, d) after pretreatment in O_2 (black), reduction with NO/NH_3 mixture (RHC, 500 ppm/600 ppm in N_2, green), subsequent oxidation with O_2 10% in N_2 (OHC, blue). The spectra in the $\delta NH_3/\delta NH_4^+$ region are background subtracted using the spectrum measured before NO/NH_3 dosage as a reference. All spectra measured at 200 °C after N_2 flush. The vertical scale of panels a) and b) is smaller than panels c) and d) by a factor of 2. (For interpretation of the references to color in this figure legend, the reader is referred to the Web version of this article.)

peaks at 950 and 896 cm^{-1} with similar intensity, indicating the presence of Z-Cu^{II}OH and Z_2Cu^{II} species in comparable amount. The presence of Z-Cu^{II}OH species at higher Si/Al ratio is expected, as the propensity of neighbouring Al^{III} ions in the framework decreases with increasing Si/Al ratio, as illustrated by a compositional phase diagram by Paolucci et al. [59]. Upon reduction in $NO/NH_3/N_2$, both the Z-Cu^{II}OH and Z_2Cu^{II} disappear, and a weaker signal around 900 cm^{-1} becomes visible upon reoxidation in O_2/N_2 at 200 °C.

The intensity of the signals for NH_3 and NH_4^+ after the NO/NH_3 treatment reflects the Cu content and Si/Al ratio, respectively. The former is like Cu-CHA with the same Cu content, while the latter is much weaker. After reoxidation, both bands are less affected with respect to the counterpart with Si/Al = 6.7: NH_3 decreases by *ca* 36% and NH_4^+ only by 5%.

The catalyst with lower Cu content at Si/Al = 6.7 shows a single peak at 900 cm^{-1} after the pretreatment in O_2 (black curve in panel d) indicating the presence of Z_2Cu^{II}, as expected, which disappears upon reduction in NO/NH_3. Reoxidation in the OHC results in a very small increase around 900 cm^{-1}, as compared to Cu-CHA with Cu/Al = 0.32 and Si/Al = 6.7, indicating that a much lower amount of Cu binds to the framework. In the δNH_3 and δNH_4^+ regions, the difference between the reduced and oxidized form of the catalyst is *ca* 31 and 5%, respectively, which is much less than observed for Cu-CHA with higher Cu loading (Cu/Al = 0.32 and Si/Al = 6.7). The disproportionate smaller changes (summarized in Table 1 as relative intensity of the bands) are in line with a lower amount of $[Cu_2^{II}(NH_3)_4(O_2)]^{2+}$species expected at low Cu density [15].

3.3. Assignment of the IR band at 900 cm^{-1}

DFT calculations were carried out on the different species potentially present in the zeolites in the tested experimental conditions. Here we consider the species presented in Fig. 5. These are framework coordinated Cu sites (Z_2Cu, Z-Cu^{II}OH, Z-Cu^{I}), NH_3 solvated Cu ions ($[Cu^{I}(NH_3)_2]^+$ and $[Cu_2^{II}(NH_3)_4O_2]^{2+}$), Brønsted acid sites and NH_4^+ ions (Z_2H_2, $Z_2(NH_4)_2$). Dimeric Cu-oxo species ($Z_2CuHOOHCu$, Z_2CuOCu, $Z_2CuOOCu$) were also considered, since these species were experimentally observed in Cu-CHA with different composition [18,64–66].

We focus our attention on the corresponding vibrational fingerprints in the silica window (Fig. 6). Framework coordinated Cu ions, Z_2Cu^{II}, Z-Cu^{II}OH and Z-Cu^{I}, result in calculated vibrations at 884, 954 and 962 cm^{-1} (bottom curves in right hand panel). These vibrations can be assigned to the Si-O ν_{sym} of framework O atom coordinating the Cu ions (see Fig. 7). The results are in good agreement with *ab initio* molecular dynamics simulations for Cu-SAPO-34 [34] and fits very well with our experimental data and with the expected higher frequency of the band related to Z-Cu^{I} [32,33,36].

To further validate our calculations, we simulated the spectra of Z_2H_2 and $Z_2(NH_4)_2$ (bottom curves in left hand panel of Fig. 6), which are not expected to perturb the $[TO_4]$ vibrations in agreement with the experimental evidence. The same holds for the mobile $[Cu^{I}(NH_3)_2]^+$ complexes (top spectra in left hand panel, light blue). Furthermore, we have calculated the vibrational fingerprint of the $[Cu_2^{II}(NH_3)_4O_2]^{2+}$ complex in the same range. In fact, some infrared studies reported νO-O bands for μ-η^2,η^2-peroxo moieties in the considered spectral range [57,67], even if it is well known that the infrared intensity for these vibrations is lower than the corresponding Raman. However, our calculations show that the $[Cu_2^{II}(NH_3)_4O_2]^{2+}$ structure has a low IR intensity for the νO-O mode, which does not show up in the 1000-800 cm^{-1} range (blue curve, in left hand panel). Finally, we considered as possible species present in the zeolites different dimeric Cu-oxo structures ($Z_2Cu^{II}HOOHCu^{II}$, $Z_2Cu^{II}O$-Cu^{II}, $Z_2Cu^{II}OOCu^{II}$), which result in vibrations with maxima around 950 cm^{-1} (top curves in right hand panel), that is close to the Z-Cu^{II}OH site. In summary, our calculations indicate that the band at 900 cm^{-1}, growing during reaction (1), can only be assigned to the Si-O ν_{sym} of the framework oxygen atoms coordinating Cu^{II} ions in the Z_2Cu^{II} species.

Table 1
Relative intensity of δNH_3 and δNH_4^+ bands in the oxidized state (10% O_2, $[Cu_2^{II}(NH_3)_4(O_2)]^{2+}$) with respect to the reduced state (NO/NH_3, $[Cu^{I}(NH_3)_2]^+$).

Cu-CHA	% δNH_3	% δNH_4^+
Cu/Al = 0.32; Si/Al = 6.7	38	68
Cu/Al = 0.62; Si/Al = 15	64	95
Cu/Al = 0.08; Si/Al = 6.7	69	95

4. Discussion

Based on the stoichiometry of reaction (1), the oxidation of $[Cu^{I}(NH_3)_2]^+$ to $[Cu_2^{II}(NH_3)_4O_2]^{2+}$, which takes place during the low

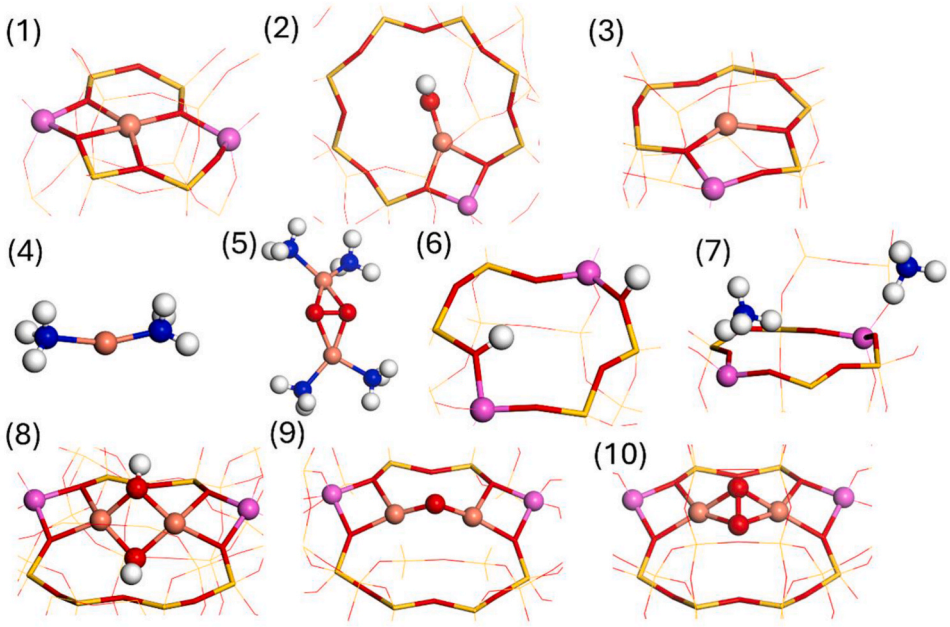

Fig. 5. Species considered for the DFT calculations: (1) Z_2Cu^{II}, (2) $ZCu^{II}OH$, (3) ZCu^{I}, (4) $[Cu^{I}(NH_3)_2]^+$ (5) $[Cu^{II}_2(NH_3)_4O_2]^{2+}$, (6) Z_2H_2, (7) $Z_2(NH_4)_2$, (8) Z_2Cu^{II}-$HOOHCu^{II}$, (9) $Z_2Cu^{II}OCu^{II}$ and (10) $Z_2Cu^{II}OOCu^{II}$. The framework is not shown for structures 4 and 5. Atomic color codes: H (white), N (blue), O (red), Al (purple), Si (yellow), and Cu (bronze). (For interpretation of the references to color in this figure legend, the reader is referred to the Web version of this article.)

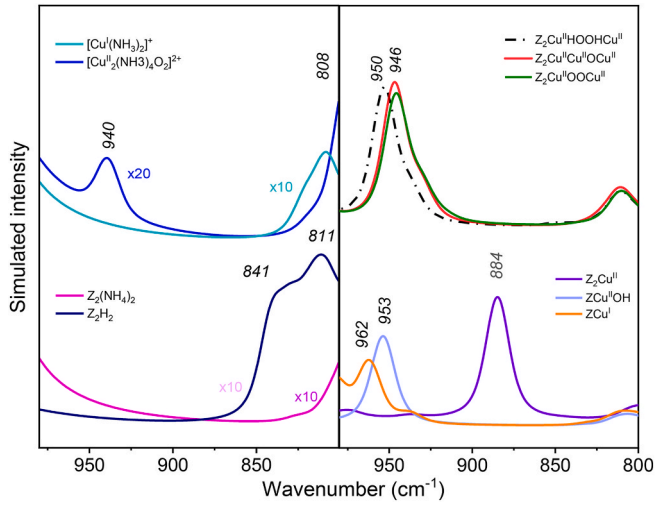

Fig. 6. Calculated IR spectra in the zeolite framework region of different counterions and electrostatically tethered Cu complexes.

temperature NH_3-SCR OHC, is not expected to result in observable changes in infrared spectroscopy, since it does not involve a change in the overall charge and number of NH_3 ligands. Our results show that in the experimental conditions probed, the reaction causes a decrease in physisorbed NH_3 and NH_4^+ groups, and the restoration of framework coordinated Cu^{II} ions, in the form of Z_2Cu^{II}.

If we assume that only reaction (1) is taking place in the probed experimental conditions, the decrease of the δNH_3 band could be explained by a loss of NH_3 ligands from the $[Cu^{II}_2(NH_3)_4O_2]^{2+}$ complexes during the OHC, which is carried out after a flushing step. In other words, the drop in the partial pressure of NH_3 could destabilize a fraction of the NH_3-solvated Cu^{II} ions, which would need to be anchored-back to the framework. Therefore, the depletion of NH_4^+ and formation of Z_2Cu^{II} sites could be described as a gas phase ion exchange, where two NH_4^+ groups are displaced by one Cu^{II} counterion. The preferential formation of Z_2Cu^{II} sites with respect to $ZCu^{II}OH$ ones can be related to their higher thermodynamical stability [64] and to the lack of OH^- ligands in the reaction atmosphere. Interestingly, the formation of Z_2Cu^{II} species during the oxidation of $[Cu^{I}(NH_3)_2]^+$ has been observed by Electron Paramagnetic Resonance (EPR) studies [68]. The same study indicated the presence of two different Z_2Cu^{II} sites in the 6-membered ring, one of which would be more favored after the oxidation of $[Cu^{I}(NH_3)_2]^+$ complexes in the OHC.

Some aspects of the process are, however, not completely understood. First, the time evolution of the bands (δNH_3, δNH_4^+ and 900 cm^{-1}, Fig. 2) indicates that Z_2Cu^{II} sites continue to grow after NH_4^+ groups are stabilized, in parallel with the decrease of NH_3 ligands. Second, during parallel XAS experiments carried out on the two Cu-CHA catalysts with Si/Al = 6.7, we did not find evidence for the release of NH_3 during the OHC (Fig. S6). This is at variance with what observed in isothermal transient kinetic response experiments on a Cu-CHA with Cu 2.4 wt% and Si/Al = 15 [69]. Our experiments instead showed the formation of H_2O, in an amount roughly proportional to the Cu loading (Fig. S6). Third, the depletion of NH_4^+ groups does not correspond to the restoration of Brønsted sites (Fig. S5). The NH_4^+ consumption is again roughly proportional to the Cu loading, in the catalysts with the same Si/Al = 6.7 (Table 1). This would suggest that H_2O is formed during the ion exchange between NH_4^+ and Cu^{II} ions, which is favored at higher Cu loading. Importantly, the formation of H_2O could explain where the protons go when we lose the Brønsted acid sites. Fourth, our observation is in apparent contradiction with the XANES results obtained on the two Cu-CHA with Si/Al = 6.7 and different Cu loadings, where an almost quantitative formation of $[Cu^{II}_2(NH_3)_4O_2]^{2+}$ complexes was observed in similar experimental conditions [39]. One possible explanation involves the presence of dimeric oxygen bridged Z_2Cu^{II} sites, with a local structure similar to that of the Cu_2O_2 core in the $[Cu^{II}_2(NH_3)_4O_2]^{2+}$ complexes, making them hardly distinguishable by XANES. This hypothesis could explain why the band at 900 cm^{-1} is broader and slightly shifted with respect to that of Z_2Cu^{II} sites in the pretreated zeolite, and could agree with the EPR observation of two distinct Z_2Cu^{II} sites [68].

From a quantitative point of view (Table 1) the exchange between NH_4^+ and Cu^{II} ions is favored at high Cu loading (3.2 wt%, Cu/Al = 0.32) and high Al density (Si/Al = 6.7). The effect is of minor entity at Si/Al = 6.7 when Cu loading is reduced (Cu/Al = 0.08), and at the same Cu

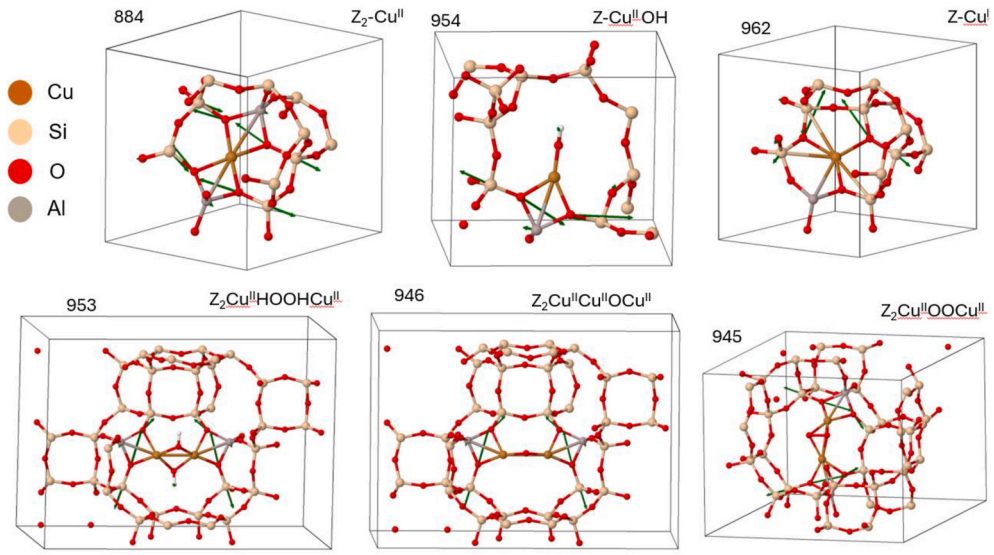

Fig. 7. Calculated normal modes of the simulated peaks at 884, 954, 962, 953, 946 and 945 cm^{-1} shown in Fig. 6. Green arrows indicate the vectors displacements. (For interpretation of the references to color in this figure legend, the reader is referred to the Web version of this article.)

loading with less Al (Si/Al = 15). Concerning Cu loading, it has been shown that the formation of $[Cu^{II}_2(NH_3)_4O_2]^{2+}$ complexes requires the vicinity of two $[Cu^{I}(NH_3)_2]^{+}$, which is favored at high Cu density [15]. Therefore, the oxidation process in the OHC is less effective on Cu-CHA with Cu/Al = 0.08 and less Cu^{II} sites are available for the ion exchange. On the other hand, it is known that the NH_3-SCR activity increases with the Al content, which is ascribed to easier paring of the $[Cu^{I}(NH_3)_2]^{+}$ complexes [19]. This could be related to the Al distribution in the framework, affecting ion diffusion in the zeolite cavities. Interestingly, recent theoretical calculations have shown a dynamical interplay between NH_4^+ and $[Cu^{I}(NH_3)_2]^{+}$ diffusion, which is influenced by the Al distribution and Cu loading [23,37]. Furthermore, the Si/Al ratio also affects the structure of the $[Cu^{II}_2(NH_3)_4O_2]^{2+}$ complexes: at low Si/Al ratio a planar Cu_2O_2 configuration is preferred, while at higher Si/Al a consistent fraction of complexes with bent Cu_2O_2 core are observed [19,70]. It could therefore be speculated that the change in the structure of the $[Cu^{II}_2(NH_3)_4O_2]^{2+}$ complexes, coupled to the influence of NH_4^+ ions on the diffusion of $[Cu^{I}(NH_3)_2]^{+}$ complexes, could influence both catalytic activity and the observed phenomenon.

On the other hand, a simple and self-consistent interpretation of the observed changes is that nitrite/nitrate species could form during the reduction step in NO/NH_3 and subsequently be consumed upon oxidation, according to the following two reactions:

$$NH_4^+ + NO_2^- \rightarrow N_2 + 2H_2O \quad (2)$$

$$H_2O + [Cu^{II}_2(NH_3)_4O_2]^{2+} \rightarrow [Cu^{II}_2(NH_3)_3(H_2O)O_2]^{2+} + NH_3 \quad (3)$$

This reaction sequence would rationalize the net formation of one equivalent of H_2O and the net consumption of one equivalent of NH_4^+, while implying the loss of one equivalent each of surface NH_4^+ and NH_3 species. The ligand exchange between H_2O and NH_3 in the $[Cu^{II}_2(NH_3)_4O_2]^{2+}$ complex could lead to its destabilization, explaining why Cu^{II} ions are moving back to a stable framework coordination.

In contrast to nitrate species, which are believed to mainly act as storage or spectator species under NO_2-rich or oxidative conditions (NO + O_2), nitrite-like intermediates (e.g. HONO) formed via Cu^{II}-pair mediated NO activation have been proposed as relevant intermediates for the reduction of NO to N_2 [40,41,71,72]. These could be formed during the RHC (NO/NH_3 mixture after pre-oxidizing the catalyst) following the reaction:

$$[Cu^{II}(NH_3)\ (OH)]^{+} + NO \rightarrow [Cu^{I}(NH_3)]^{+} + HONO \quad (4)$$

And subsequently react with NH_3:

$$HONO \rightleftarrows NO + NO_2 + H_2O \quad (5)$$

Reaction (5) is very fast, so that the kinetically labile HONO intermediate could only be probed indirectly, by transient response methods or by chemical trapping followed by TPD [41].

In the experiments described in this work, we did not observe nitrates formation, and we can neither confirm nor exclude the hypothesis that what we observe is due the oxidation of nitrites formed in the RHC. The evolution with time of the bands related to NH_4^+, NH_3 and Z_2Cu^{II} (Fig. 2c) could agree with the consecutive reactions outlined in Eqs. (2) and (3). However, we could not observe a quantitative formation of N_2 in our parallel experiments (not reported), which would be expected on the basis of Eq. (2). In any case, our results indicate a consumption of NH_4^+ ions which are electrostatically compensated by the coordination of Cu^{II} ions to the framework. This could be the consequence of the instability of the $[Cu^{II}_2(NH_3)_3(H_2O)O_2]^{2+}$ complex formed in Eq. (3).

5. Conclusions

The exposure of Cu-CHA catalysts to an NH_3/NO atmosphere at 200 °C in the RHC causes the formation of $[Cu^{I}(NH_3)_2]^{+}$ complexes, which are characterized in infrared spectroscopy by the δNH_3 band at 1620 cm^{-1} and by the disappearance of the framework coordinated Z_2Cu^{II} and $ZCu^{II}OH$ fingerprints at 896 and 950 cm^{-1}, respectively. The subsequent oxidation (OHC) causes the formation of the $[Cu^{II}_2(NH_3)_4O_2]^{2+}$ peroxo complexes, which are relevant intermediates in the low temperature NH_3-SCR reaction. Following this reaction, we observed an unexpected decrease in the concentration of NH_3 ligands and of NH_4^+ (formed by protonation of NH_3 by the residual Brønsted sites), concomitant to the growth of a band at 900 cm^{-1}. Thanks to DFT calculations we can safely relate this band to newly formed Z_2Cu^{II} sites. This indicates that during the isothermal formation of the $[Cu^{II}_2(NH_3)_4O_2]^{2+}$ complexes one fraction of Cu^{II} ions loses NH_3 ligands and is again coordinated by the framework. Charge compensation implies that NH_4^+ needs to be displaced by Cu^{II}, with formation of H_2O that is likely responsible for the removal of Brønsted acid sites. The observed consumption of NH_4^+ and NH_3 during the OHC could be explained by the oxidation of (IR silent) nitrite species formed during the RHC. Our results would imply that the $[Cu^{II}_2(NH_3)_3(H_2O)O_2]^{2+}$ complex formed in this reaction would be unstable, leading to the removal of NH_3 and H_2O ligands with consequent coordination of Cu^{II} ions to the framework. In

this case our observations could be explained as a combination of an NH_3-SCR-type reaction occurring alongside a change in Cu complex speciation due to ligand replacement and ion-exchange.

The observed changes are more important in the Cu-CHA catalyst with high Cu loading and Al density (3.2 wt%, Cu/Al = 0.32 and Si/Al = 6.7), while they are comparable at lower Cu loading (0.8 wt%, Cu/Al = 0.08 and Si/Al = 6.7) or at higher Si/Al ratio (Cu 3.2 wt%, Cu/Al = 0.62 and Si/Al = 15). Therefore, the larger difference in infrared intensity for the reduced and oxidized states is caused by a larger fraction of framework-bound Cu^{II} upon oxidation, leading to less NH_3 and NH_4^+ in the catalyst. It has been previously shown that both Cu content and Si/Al influence the migration of $[Cu^{I}(NH_3)_2]^+$ complexes, which in turns affects the capacity of the catalyst to be oxidized to $[Cu^{II}_2(NH_3)_4O_2]^{2+}$ complexes. On the other hand, the Si/Al ratio influences the speciation between different configurations (planar or bent Cu_2O_2 core) of the $[Cu^{II}_2(NH_3)_4O_2]^{2+}$ complexes, which could influence their reducibility and consequently the catalytic activity. Our results suggest that the formation of framework bound Cu^{II} sites is higher in the catalysts where the formation of $[Cu^{II}_2(NH_3)_4O_2]^{2+}$ complexes is expected to be higher, and preferably in the planar configuration. Moreover, it shows an interplay between the diffusion of Cu and NH_4^+ ions, in agreement with theoretical predictions. Finally, the framework coordination of Z_2Cu^{II} sites is seen to be favourable with respect to Z-Cu^{II}OH sites irrespective of the zeolite composition, which could shed some light on the debate about the different catalytic activity of these two sites.

CRediT authorship contribution statement

Stefano Magliocco: Writing – original draft, Investigation, Data curation. **Reza K. Abasabadi:** Writing – review & editing, Conceptualization. **Francesco D'Amico:** Writing – review & editing, Data curation. **Joachim D. Bjerregaard:** Investigation. **Anastasia Yu Molokova:** Writing – review & editing. **Henrik Grönbeck:** Writing – review & editing. **Ton V.W. Janssens:** Writing – review & editing. **Gloria Berlier:** Writing – review & editing, Supervision, Project administration, Data curation, Conceptualization.

Declaration of AI use

During the preparation of this work the authors used ChatGPT 5.1 Thinking in order to generate the cage image (grey) in the graphical abstract. After using this tool/service, the authors reviewed and edited the content as needed and take full responsibility for the content of the published article.

Declaration of competing interest

The authors declare the following financial interests/personal relationships which may be considered as potential competing interests: Gloria Berlier reports financial support was provided by European Commission. If there are other authors, they declare that they have no known competing financial interests or personal relationships that could have appeared to influence the work reported in this paper.

Acknowledgements

We acknowledge support from the European Union's Horizon 2020 Research and Innovation Programme under the Marie Sklodowska-Curie grant agreement No. 955839 (CHASS) and from the Project CH4.0 under the MUR program “Dipartimenti di Eccellenza 2023-2027” (CUP: D13C22003520001). We also acknowledge the ESRF for the allocation of beamtime at BM23 beamline (experiment CH-6662), during which the mass-spectrometry data reported in the SI were collected. The calculations have been performed at C3SE (Göteborg) and NSC (Linköping) through a NAISS grant.

Appendix A. Supplementary data

Supplementary data to this article can be found online at https://doi.org/10.1016/j.micromeso.2026.114075.

Data availability

Data will be made available on request.

References

[1] C.K. Lambert, Perspective on SCR NOx control for diesel vehicles, React. Chem. Eng. 4 (2019) 969–974, https://doi.org/10.1039/C8RE00284C.
[2] E. Borfecchia, P. Beato, S. Svelle, U. Olsbye, C. Lamberti, S. Bordiga, Cu-CHA – a model system for applied selective redox catalysis, Chem. Soc. Rev. 47 (2018) 8097–8133, https://doi.org/10.1039/C8CS00373D.
[3] W. Hu, T. Selleri, F. Gramigni, E. Fenes, K.R. Rout, S. Liu, I. Nova, D. Chen, X. Gao, E. Tronconi, On the redox mechanism of low-temperature NH_3 -SCR over Cu-CHA: a combined experimental and theoretical study of the reduction half cycle, Angew. Chem. Int. Ed. 60 (2021) 7197–7204, https://doi.org/10.1002/anie.202014926.
[4] W. Hu, F. Gramigni, N.D. Nasello, N. Usberti, U. Iacobone, S. Liu, I. Nova, X. Gao, E. Tronconi, Dynamic binuclear Cu^{II} sites in the reduction half-cycle of low-temperature NH_3 –SCR over Cu-CHA catalysts, ACS Catal. 12 (2022) 5263–5274, https://doi.org/10.1021/acscatal.2c01213.
[5] Y. Feng, X. Wang, T.V.W. Janssens, P.N.R. Vennestrøm, J. Jansson, M. Skoglundh, H. Grönbeck, First-principles microkinetic model for low-temperature NH $_3$ -Assisted selective catalytic reduction of NO over Cu-CHA, ACS Catal. 11 (2021) 14395–14407, https://doi.org/10.1021/acscatal.1c03973.
[6] N.D. Nasello, N. Usberti, U. Iacobone, F. Gramigni, W. Hu, S. Liu, I. Nova, X. Gao, E. Tronconi, Dual-site RHC and OHC transient kinetics predict Low-T standard SCR steady-state rates over a Cu-CHA catalyst, ACS Catal. 13 (2023) 2723–2734, https://doi.org/10.1021/acscatal.2c06071.
[7] F. Gramigni, N.D. Nasello, N. Usberti, U. Iacobone, T. Selleri, W. Hu, S. Liu, X. Gao, I. Nova, E. Tronconi, Transient kinetic analysis of low-temperature NH_3 -SCR over Cu-CHA catalysts reveals a quadratic dependence of Cu reduction rates on Cu^{II}, ACS Catal. 11 (2021) 4821–4831, https://doi.org/10.1021/acscatal.0c05362.
[8] A. Marberger, A.W. Petrov, P. Steiger, M. Elsener, O. Kröcher, M. Nachtegaal, D. Ferri, Time-resolved copper speciation during selective catalytic reduction of NO on Cu-SSZ-13, Nat. Catal. 1 (2018) 221–227, https://doi.org/10.1038/s41929-018-0032-6.
[9] Y. Zhang, Y. Peng, K. Li, S. Liu, J. Chen, J. Li, F. Gao, C.H.F. Peden, Using transient FTIR spectroscopy to probe active sites and reaction intermediates for selective catalytic reduction of NO on Cu/SSZ-13 catalysts, ACS Catal. 9 (2019) 6137–6145, https://doi.org/10.1021/acscatal.9b00759.
[10] F. Gao, D. Mei, Y. Wang, J. Szanyi, C.H.F. Peden, Selective catalytic reduction over Cu/SSZ-13: linking Homo- and heterogeneous catalysis, J. Am. Chem. Soc. 139 (2017) 4935–4942, https://doi.org/10.1021/jacs.7b01128.
[11] L. Chen, T.V.W. Janssens, P.N.R. Vennestrøm, J. Jansson, M. Skoglundh, H. Grönbeck, A complete multisite reaction mechanism for low-temperature NH3-SCR over Cu-CHA, ACS Catal. 10 (2020) 5646–5656, https://doi.org/10.1021/acscatal.0c00440.
[12] T.V.W. Janssens, H. Falsig, L.F. Lundegaard, P.N.R. Vennestrøm, S.B. Rasmussen, P. G. Moses, F. Giordanino, E. Borfecchia, K.A. Lomachenko, C. Lamberti, S. Bordiga, A. Godiksen, S. Mossin, P. Beato, A consistent reaction scheme for the selective catalytic reduction of nitrogen oxides with ammonia, ACS Catal. 5 (2015) 2832–2845, https://doi.org/10.1021/cs501673g.
[13] N.D. Nasello, U. Iacobone, N. Usberti, A. Gjetja, I. Nova, E. Tronconi, R. Villamaina, M.P. Ruggeri, D. Bounechada, A.P.E. York, J. Collier, Investigation of low-temperature OHC and RHC in NH_3 –SCR over Cu-CHA catalysts: effects of H_2 O and SAR, ACS Catal. 14 (2024) 4265–4276, https://doi.org/10.1021/acscatal.4c00118.
[14] F. Giordanino, E. Borfecchia, K.A. Lomachenko, A. Lazzarini, G. Agostini, E. Gallo, A.V. Soldatov, P. Beato, S. Bordiga, C. Lamberti, Interaction of NH $_3$ with Cu-SSZ-13 catalyst: a complementary FTIR, XANES, and XES study, J. Phys. Chem. Lett. 5 (2014) 1552–1559, https://doi.org/10.1021/jz500241m.
[15] C. Paolucci, I. Khurana, A.A. Parekh, S. Li, A.J. Shih, H. Li, J.R. Di Iorio, J. D. Albarracin-Caballero, A. Yezerets, J.T. Miller, W.N. Delgass, F.H. Ribeiro, W. F. Schneider, R. Gounder, Dynamic multinuclear sites formed by mobilized copper ions in NO $_x$ selective catalytic reduction, Science 357 (2017) 898–903, https://doi.org/10.1126/science.aan5630.
[16] S. Shwan, M. Skoglundh, L.F. Lundegaard, R.R. Tiruvalam, T.V.W. Janssens, A. Carlsson, P.N.R. Vennestrøm, Solid-state ion-exchange of copper into zeolites facilitated by ammonia at low temperature, ACS Catal. 5 (2015) 16–19, https://doi.org/10.1021/cs5015139.
[17] K.A. Lomachenko, E. Borfecchia, C. Negri, G. Berlier, C. Lamberti, P. Beato, H. Falsig, S. Bordiga, The Cu-CHA deNO x catalyst in action: temperature-dependent NH 3 -Assisted selective catalytic reduction monitored by operando XAS and XES, J. Am. Chem. Soc. 138 (2016) 12025–12028, https://doi.org/10.1021/jacs.6b06809.
[18] C. Negri, T. Selleri, E. Borfecchia, A. Martini, K.A. Lomachenko, T.V.W. Janssens, M. Cutini, S. Bordiga, G. Berlier, Structure and reactivity of oxygen-bridged diamino Dicopper(II) complexes in cu-ion-exchanged chabazite catalyst for NH 3

-Mediated selective catalytic reduction, J. Am. Chem. Soc. 142 (2020) 15884–15896, https://doi.org/10.1021/jacs.0c06270.
[19] T.V.W. Janssens, E. Borfecchia, K.A. Lomachenko, H. Grönbeck, G. Berlier, The [(NH3)4 Cu2 O2]2+ -peroxo complex as the key intermediate for NH3 -SCR activity and deactivation of Cu-CHA catalysts, ChemCatChem 16 (2024) e202400384, https://doi.org/10.1002/cctc.202400384.
[20] S.H. Krishna, A. Goswami, Y. Wang, C.B. Jones, D.P. Dean, J.T. Miller, W. F. Schneider, R. Gounder, Influence of framework Al density in chabazite zeolites on copper ion mobility and reactivity during NOx selective catalytic reduction with NH3, Nat. Catal. 6 (2023) 276–285, https://doi.org/10.1038/s41929-023-00932-5.
[21] R. Millan, E. Bello-Jurado, M. Moliner, M. Boronat, R. Gomez-Bombarelli, Effect of framework composition and NH 3 on the diffusion of Cu + in Cu-CHA catalysts predicted by machine-learning accelerated molecular dynamics, ACS Cent. Sci. 9 (2023) 2044–2056, https://doi.org/10.1021/acscentsci.3c00870.
[22] Y. Fu, W. Ding, H. Lei, Y. Sun, J. Du, Y. Yu, U. Simon, P. Chen, Y. Shan, G. He, H. He, Spatial distribution of brønsted acid sites determines the mobility of reactive Cu ions in the Cu-SSZ-13 catalyst during the selective catalytic reduction of NO x with NH3, J. Am. Chem. Soc. 146 (2024) 11141–11151, https://doi.org/10.1021/jacs.3c13725.
[23] J.D. Bjerregaard, M. Votsmeier, H. Grönbeck, Influence of aluminium distribution on the diffusion mechanisms and pairing of [Cu(NH3)2]+ complexes in Cu-CHA, Nat. Commun. 16 (2025) 603, https://doi.org/10.1038/s41467-025-55859-1.
[24] F. Gao, E.D. Walter, M. Kollar, Y. Wang, J. Szanyi, C.H.F. Peden, Understanding ammonia selective catalytic reduction kinetics over Cu/SSZ-13 from motion of the Cu ions, J. Catal. 319 (2014) 1–14, https://doi.org/10.1016/j.jcat.2014.08.010.
[25] F. Gao, E.D. Walter, E.M. Karp, J. Luo, R.G. Tonkyn, J.H. Kwak, J. Szanyi, C.H. F. Peden, Structure–activity relationships in NH3-SCR over Cu-SSZ-13 as probed by reaction kinetics and EPR studies, J. Catal. 300 (2013) 20–29, https://doi.org/10.1016/j.jcat.2012.12.020.
[26] A.G. Greenaway, A. Marberger, A. Thetford, I. Lezcano-González, M. Agote-Arán, M. Nachtegaal, D. Ferri, O. Kröcher, C.R.A. Catlow, A.M. Beale, Detection of key transient Cu intermediates in SSZ-13 during NH3 -SCR deNOx by modulation excitation IR spectroscopy, Chem. Sci. 11 (2020) 447–455, https://doi.org/10.1039/C9SC04905C.
[27] C. Tyrsted, E. Borfecchia, G. Berlier, K.A. Lomachenko, C. Lamberti, S. Bordiga, P. N.R. Vennestrøm, T.V.W. Janssens, H. Falsig, P. Beato, A. Puig-Molina, Nitrate–nitrite equilibrium in the reaction of NO with a Cu-CHA catalyst for NH3 -SCR, Catal. Sci. Technol. 6 (2016) 8314–8324, https://doi.org/10.1039/C6CY01820C.
[28] C. Negri, P.S. Hammershøi, T.V.W. Janssens, P. Beato, G. Berlier, S. Bordiga, Investigating the low temperature formation of CuII -(N,O) species on Cu-CHA zeolites for the selective catalytic reduction of NOx, Chem. Eur J. 24 (2018) 12044–12053, https://doi.org/10.1002/chem.201802769.
[29] S. Bordiga, L. Regli, C. Lamberti, A. Zecchina, M. Bjørgen, K.P. Lillerud, FTIR adsorption studies of H2O and CH3OH in the isostructural H-SSZ-13 and H-SAPO-34: formation of H-Bonded adducts and protonated clusters, J. Phys. Chem. B 109 (2005) 7724–7732, https://doi.org/10.1021/jp044324b.
[30] J. Luo, D. Wang, A. Kumar, J. Li, K. Kamasamudram, N. Currier, A. Yezerets, Identification of two types of Cu sites in Cu/SSZ-13 and their unique responses to hydrothermal aging and sulfur poisoning, Catal. Today 267 (2016) 3–9, https://doi.org/10.1016/j.cattod.2015.12.002.
[31] J. Luo, F. Gao, K. Kamasamudram, N. Currier, C.H.F. Peden, A. Yezerets, New insights into Cu/SSZ-13 SCR catalyst acidity. Part I: nature of acidic sites probed by NH3 titration, J. Catal. 348 (2017) 291–299, https://doi.org/10.1016/j.jcat.2017.02.025.
[32] E. Groppo, S. Rojas-Buzo, S. Bordiga, The role of in situ/operando IR spectroscopy in unraveling adsorbate-induced structural changes in heterogeneous catalysis, Chem. Rev. 123 (2023) 12135–12169, https://doi.org/10.1021/acs.chemrev.3c00372.
[33] J. Hun Kwak, H. Zhu, J.H. Lee, C.H.F. Peden, J. Szanyi, Two different cationic positions in Cu-SSZ-13? Chem. Commun. 48 (2012) 4758, https://doi.org/10.1039/c2cc31184d.
[34] R. Millan, P. Cnudde, A.E.J. Hoffman, C.W. Lopes, P. Concepción, V. Van Speybroeck, M. Boronat, Theoretical and spectroscopic evidence of the dynamic nature of copper active sites in Cu-CHA catalysts under selective catalytic reduction (NH 3 –SCR–NO x) conditions, J. Phys. Chem. Lett. 11 (2020) 10060–10066, https://doi.org/10.1021/acs.jpclett.0c03020.
[35] Y. Jangjou, Q. Do, Y. Gu, L.-G. Lim, H. Sun, D. Wang, A. Kumar, J. Li, L.C. Grabow, W.S. Epling, Nature of Cu active centers in Cu-SSZ-13 and their responses to SO 2 exposure, ACS Catal. 8 (2018) 1325–1337, https://doi.org/10.1021/acscatal.7b03095.
[36] J.H. Kwak, T. Varga, C.H.F. Peden, F. Gao, J.C. Hanson, J. Szanyi, Following the movement of Cu ions in a SSZ-13 zeolite during dehydration, reduction and adsorption: a combined in situ TP-XRD, XANES/DRIFTS study, J. Catal. 314 (2014) 83–93, https://doi.org/10.1016/j.jcat.2014.03.003.
[37] R.K. Abasabadi, T.V.W. Janssens, S. Bordiga, G. Berlier, Probing the effect of the Si/Al ratio in Cu-CHA zeolite catalysts on SO 2 exposure: in situ DR UV-vis spectroscopy and deactivation measurements, Catal. Sci. Technol. 14 (2024) 3076–3085, https://doi.org/10.1039/D4CY00129J.
[38] A.Yu Molokova, E. Borfecchia, A. Martini, I.A. Pankin, C. Atzori, O. Mathon, S. Bordiga, F. Wen, P.N.R. Vennestrøm, G. Berlier, T.V.W. Janssens, K. A. Lomachenko, SO 2 poisoning of Cu-CHA deNO x catalyst: the Most vulnerable Cu species identified by X-ray absorption spectroscopy, JACS Au 2 (2022) 787–792, https://doi.org/10.1021/jacsau.2c00053.
[39] A.Yu Molokova, R.K. Abasabadi, E. Borfecchia, O. Mathon, S. Bordiga, F. Wen, G. Berlier, T.V.W. Janssens, K.A. Lomachenko, Elucidating the reaction mechanism of SO 2 with Cu-CHA catalysts for NH 3 -SCR by X-ray absorption spectroscopy, Chem. Sci. 14 (2023) 11521–11531, https://doi.org/10.1039/D3SC03924B.
[40] N. Usberti, F. Gramigni, N.D. Nasello, U. Iacobone, T. Selleri, W. Hu, S. Liu, X. Gao, I. Nova, E. Tronconi, An experimental and modelling study of the reactivity of adsorbed NH3 in the low temperature NH3-SCR reduction half-cycle over a Cu-CHA catalyst, Appl. Catal. B Environ. 279 (2020) 119397, https://doi.org/10.1016/j.apcatb.2020.119397.
[41] W. Hu, F. Gramigni, N.D. Nasello, N. Usberti, U. Iacobone, S. Liu, I. Nova, X. Gao, E. Tronconi, Dynamic binuclear CuII sites in the reduction half-cycle of low-temperature NH3 –SCR over Cu-CHA catalysts, ACS Catal. 12 (2022) 5263–5274, https://doi.org/10.1021/acscatal.2c01213.
[42] M. Signorile, E. Borfecchia, S. Bordiga, G. Berlier, Influence of ion mobility on the redox and catalytic properties of Cu ions in zeolites, Chem. Sci. 13 (2022) 10238–10250, https://doi.org/10.1039/D2SC03565K.
[43] Chemistry A European J - 2012 - Wuttke - Discovering the Active Sites for C3 Separation in MIL-100 Fe by Using Operando IR, (n.d.).
[44] G. Kresse, J. Furthmüller, Efficient iterative schemes for ab initio total-energy calculations using a plane-wave basis set, Phys. Rev. B 54 (1996) 11169–11186, https://doi.org/10.1103/PhysRevB.54.11169.
[45] G. Kresse, J. Hafner, Ab initio molecular-dynamics simulation of the liquid-metal–amorphous-semiconductor transition in germanium, Phys. Rev. B 49 (1994) 14251–14269, https://doi.org/10.1103/PhysRevB.49.14251.
[46] J.P. Perdew, K. Burke, M. Ernzerhof, Generalized gradient approximation made simple, Phys. Rev. Lett. 77 (1996) 3865–3868, https://doi.org/10.1103/PhysRevLett.77.3865.
[47] S. Grimme, J. Antony, S. Ehrlich, H. Krieg, A consistent and accurate ab initio parametrization of density functional dispersion correction (DFT-D) for the 94 elements H-Pu, J. Chem. Phys. 132 (2010) 154104, https://doi.org/10.1063/1.3382344.
[48] S.L. Dudarev, G.A. Botton, S.Y. Savrasov, C.J. Humphreys, A.P. Sutton, Electron-energy-loss spectra and the structural stability of nickel oxide: an LSDA+U study, Phys. Rev. B 57 (1998) 1505–1509, https://doi.org/10.1103/PhysRevB.57.1505.
[49] P.E. Blöchl, Projector augmented-wave method, Phys. Rev. B 50 (1994) 17953–17979, https://doi.org/10.1103/PhysRevB.50.17953.
[50] G. Kresse, D. Joubert, From ultrasoft pseudopotentials to the projector augmented-wave method, Phys. Rev. B 59 (1999) 1758–1775, https://doi.org/10.1103/PhysRevB.59.1758.
[51] D. Karhánek, dakarhanek/VASP-infrared-intensities: VASP-infrared-intensities. https://doi.org/10.5281/ZENODO.3930989, 2020.
[52] A. Fonari, S. Stauffer, Vasp_raman.py. https://github.com/raman-sc/VASP/, 2013.
[53] M.K. Kesharwani, B. Brauer, J.M.L. Martin, Frequency and zero-point vibrational energy scale factors for double-hybrid density functionals (and other selected methods): can anharmonic force fields be avoided? J. Phys. Chem. A 119 (2015) 1701–1714, https://doi.org/10.1021/jp508422u.
[54] F. D'Amico, M.E. Musso, R.J.F. Berger, N. Cefarin, G. Birarda, G. Tondi, D. Bertoldo Menezes, A. Reyer, L. Scarabattoli, T. Sepperer, T. Schnabel, L. Vaccari, Chemical constitution of polyfurfuryl alcohol investigated by FTIR and resonant raman spectroscopy, Spectrochim. Acta. A. Mol. Biomol. Spectrosc. 262 (2021) 120090, https://doi.org/10.1016/j.saa.2021.120090.
[55] K. Barbera, F. Bonino, S. Bordiga, T.V.W. Janssens, P. Beato, Structure–deactivation relationship for ZSM-5 catalysts governed by framework defects, J. Catal. 280 (2011) 196–205, https://doi.org/10.1016/j.jcat.2011.03.016.
[56] F. Giordanino, P.N.R. Vennestrøm, L.F. Lundegaard, F.N. Stappen, S. Mossin, P. Beato, S. Bordiga, C. Lamberti, Characterization of Cu-exchanged SSZ-13: a comparative FTIR, UV-Vis, and EPR study with Cu-ZSM-5 and Cu-β with similar Si/Al and Cu/Al ratios, Dalton Trans. 42 (2013) 12741–12761, https://doi.org/10.1039/C3DT50732G.
[57] K. Mudiyanselage, H. Idriss, Characterization of peroxo species on TiO/Rh(111) single crystal, Surf. Sci. 680 (2019) 61–67, https://doi.org/10.1016/j.susc.2018.10.014.
[58] M. Ravi, V.L. Sushkevich, J.A. Van Bokhoven, On the location of lewis acidic aluminum in zeolite mordenite and the role of framework-associated aluminum in mediating the switch between Brønsted and Lewis acidity, Chem. Sci. 12 (2021) 4094–4103, https://doi.org/10.1039/D0SC06130A.
[59] C. Paolucci, A.A. Parekh, I. Khurana, J.R. Di Iorio, H. Li, J.D. Albarracin Caballero, A.J. Shih, T. Anggara, W.N. Delgass, J.T. Miller, F.H. Ribeiro, R. Gounder, W. F. Schneider, Catalysis in a cage: Condition-dependent speciation and dynamics of exchanged Cu cations in SSZ-13 zeolites, J. Am. Chem. Soc. 138 (2016) 6028–6048, https://doi.org/10.1021/jacs.6b02651.
[60] A. Zecchina, L. Marchese, S. Bordiga, C. Pazè, E. Gianotti, Vibrational spectroscopy of NH4+ ions in zeolitic materials: an IR study, J. Phys. Chem. B 101 (1997) 10128–10135, https://doi.org/10.1021/jp9717554.
[61] A.A. Tsyganenko, D.V. Pozdnyakov, V.N. Filimonov, Infrared study of surface species arising from ammonia adsorption on oxide surfaces, J. Mol. Struct. 29 (1975) 299–318, https://doi.org/10.1016/0022-2860(75)85038-1.
[62] Y. Ganjkhanlou, T.V.W. Janssens, P.N.R. Vennestrøm, L. Mino, M.C. Paganini, M. Signorile, S. Bordiga, G. Berlier, Location and activity of VOx species on TiO2 particles for NH3-SCR catalysis, Appl. Catal. B Environ. 278 (2020) 119337, https://doi.org/10.1016/j.apcatb.2020.119337.
[63] B. Onida, F. Geobaldo, F. Testa, F. Crea, E. Garrone, FTIR investigation of the interaction at 77 K of diatomic molecular probes on MCM-22 zeolite, Microporous Mesoporous Mater. 30 (1999) 119–127, https://doi.org/10.1016/S1387-1811(99)00033-5.

[64] H. Li, C. Paolucci, I. Khurana, L.N. Wilcox, F. Göltl, J.D. Albarracin-Caballero, A. J. Shih, F.H. Ribeiro, R. Gounder, W.F. Schneider, Consequences of exchange-site heterogeneity and dynamics on the UV-visible spectrum of Cu-exchanged SSZ-13, Chem. Sci. 10 (2019) 2373–2384, https://doi.org/10.1039/C8SC05056B.

[65] C. Negri, M. Signorile, N.G. Porcaro, E. Borfecchia, G. Berlier, T.V.W. Janssens, S. Bordiga, Dynamic CuII/CuI speciation in Cu-CHA catalysts by in situ diffuse reflectance UV–vis-NIR spectroscopy, Appl. Catal. Gen. 578 (2019) 1–9, https://doi.org/10.1016/j.apcata.2019.03.018.

[66] C. Negri, A. Martini, G. Deplano, K.A. Lomachenko, T.V.W. Janssens, E. Borfecchia, G. Berlier, S. Bordiga, Investigating the role of Cu-oxo species in Cu-nitrate formation over Cu-CHA catalysts, Phys. Chem. Chem. Phys. 23 (2021) 18322–18337, https://doi.org/10.1039/D1CP01754C.

[67] G.G. Martirosyan, A.A. Hovhannisyan, A.V. Iretskii, Mechanism of autoxidation of the chromium(II) porphyrins. In situ infrared spectroscopic detection of the peroxo- intermediate, Inorg. Chim. Acta. 566 (2024) 122031, https://doi.org/10.1016/j.ica.2024.122031.

[68] A. Godiksen, O.L. Isaksen, S.B. Rasmussen, P.N.R. Vennestrøm, S. Mossin, Site-specific reactivity of copper chabazite zeolites with nitric oxide, ammonia, and oxygen, ChemCatChem 10 (2018) 366–370, https://doi.org/10.1002/cctc.201701357.

[69] R. Daya, D. Trandal, U. Menon, D.J. Deka, W.P. Partridge, S.Y. Joshi, Kinetic model for the reduction of CuII sites by NO + NH3 and reoxidation of NH3 -Solvated CuI sites by O2 and NO in Cu-SSZ-13, ACS Catal. 12 (2022) 6418–6433, https://doi.org/10.1021/acscatal.2c01076.

[70] A. Martini, C. Negri, L. Bugarin, G. Deplano, R.K. Abasabadi, K.A. Lomachenko, T. V.W. Janssens, S. Bordiga, G. Berlier, E. Borfecchia, Assessing the influence of zeolite composition on oxygen-bridged diamino Dicopper(II) complexes in Cu-CHA DeNO x catalysts by machine learning-assisted X-ray absorption spectroscopy, J. Phys. Chem. Lett. 13 (2022) 6164–6170, https://doi.org/10.1021/acs.jpclett.2c01107.

[71] U. Iacobone, N.D. Nasello, I. Nova, E. Tronconi, R. Daya, H. An, U. Menon, Assessing Cu2+ active sites evolution on Cu-SSZ-13 NH3-SCR catalysts during hydrothermal aging: a transient response approach, Appl. Catal. B Environ. Energy 351 (2024) 123989, https://doi.org/10.1016/j.apcatb.2024.123989.

[72] W. Hu, T. Selleri, F. Gramigni, E. Fenes, K.R. Rout, S. Liu, I. Nova, D. Chen, X. Gao, E. Tronconi, On the redox mechanism of low-temperature NH3 -SCR over Cu-CHA: a combined experimental and theoretical study of the reduction half cycle, Angew. Chem. Int. Ed. 60 (2021) 7197–7204, https://doi.org/10.1002/anie.202014926.